Deep Dehazing Powered by Image Processing Network

Guisik Kim[1], Jinhee Park[2], and Junseok Kwon[2]
[1]Korea Electronics Technology Institute
[2]School of Computer Science and Engineering, Chung-Ang University, Seoul, Korea
specialre@naver.com iv4084em@gmail.com jskwon@cau.ac.kr

Abstract

*Image processing is a very fundamental technique in the field of low-level vision. However, with the development of deep learning over the past five years, most low-level vision methods tend to ignore this technique. Recent dehazing methods also refrain from using conventional image processing techniques, whereas only focusing on the development of new deep neural network (DNN) architectures. Unlike this recent trend, we show that image processing techniques are still competitive, if they are incorporated into DNNs. In this paper, we utilize conventional image processing techniques (*i.e. *curve adjustment, retinex decomposition, and multiple image fusion) for accurate dehazing. Moreover, we employ direct learning for stable dehazing performance. The proposed method can perform with low computational cost and easy to learn. The experimental results demonstrate that the proposed method produces accurate dehazing results compared to recent algorithms.*

1. Introduction

Image processing is a common technique of processing images. By applying this image processing technique, most low-level vision methods that deal with pixel values directly (*e.g.* deraining, dehazing and low-light enhancement) can achieve high performance. Nevertheless, due to the development of deep learning, image processing techniques have been easily ignored in the computer vision community and the corresponding researches have decreased gradually.

Dehazing is a representative task using image processing and one of fundamental problems in computer vision, which aims to recover haze-free images from haze images. While it has been actively researched with various approaches, recent dehazing methods have achieved a great success in terms of accuracy with the aid of deep learning. The haze model is typically described as follows.

$$I(x) = J(x)t(x) + A\left(1 - t(x)\right), \tag{1}$$

where the haze image I is described as an weighted linear combination of the haze-free image J and the atmosphere A at each pixel coordinate x. The weight is determined using the transmission t. Due to the lack of training data, deep learning-based dehazing methods typically synthesize haze regions using the aforementioned haze model in (1). In particular, transformer and flow model-based dehazing methods with sophisticated deep neural architectures [20, 27] enable to extract representative haze features and produce accurate dehazing results. Thus, image processing-based [15, 41] or prior-based haze methods [9, 16, 21]) have been rarely studied in these days, because they have difficulty in outperforming deep learning-based methods. Recent dehazing methods refrain from using conventional image processing techniques, whereas only focusing on the development of new deep neural network (DNN) architectures. Although image processing techniques are helpful for improving the performance, few studies apply these techniques to DNNs.

In this paper, we argue that image processing can be used as a prior for DNNs to maintain proper characteristics of the dehazing task. We complete the aforementioned argument through several experiments, in which each image processing technique differently contributes the improvement of the dehazing accuracy and their combination induces the best accuracy. For this, we adopt conventional image processing techniques, which are curve adjustment, retinex decomposition, and image fusion modules. Each image processing module can be designed using simple layers, while still showing high performance.

In particular, the curve adjustment is an image processing technique that is widely used in commercial photo editing applications (*e.g.* Adobe Lightroom and Photoshop) to adjust the brightness and tone of an image to generate differently stylized images. Moran *et al.* [34] and Guo *et al.* [19] solved image enhancement and low-light enhancement problems using this curve adjustment technique, respectively. The retinex decomposition is an image processing technique that is widely used in low-light enhancement [28, 38, 43, 45] to describe an image using reflectance and illumination components. The image fusion is an image processing technique to combine multiple images with different properties [50]. Fig.1 shows the whole pipeline of

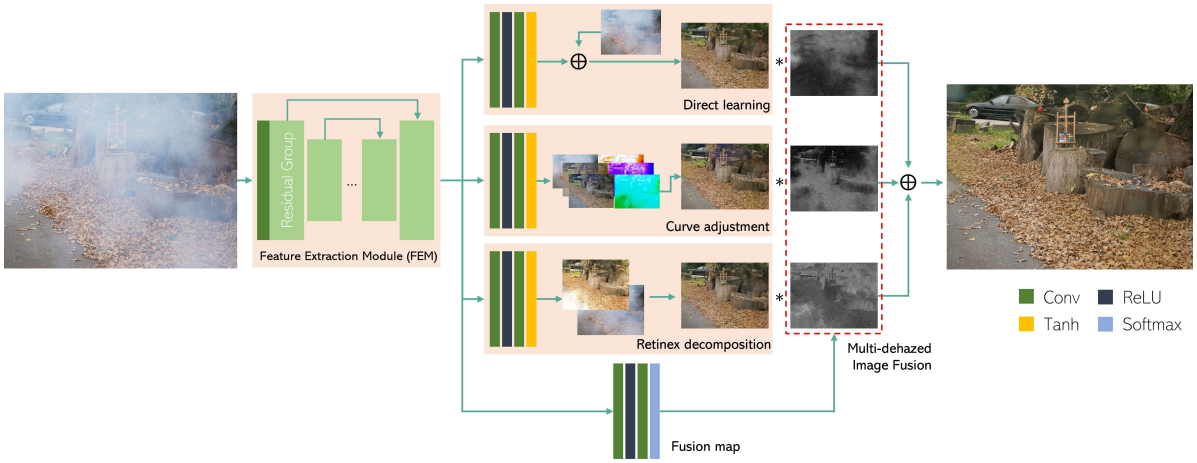

Figure 1. **Overview of the proposed method.** For dehazing, the proposed method extracts features using the feature extraction module (FEM). Subsequently, it conducts direct learning, pixel-wise curve adjustment, and retinex decomposition, which produce three intermediate dehazing results. By fusing these results, the proposed method obtains final dehazing results.

our method. Our contributions are as follows.

• We demonstrate that incorporating simple image processing techniques, such as curve adjustment, retinex decomposition, and image fusion, into the network yields competitive results compared to recent complex networks for dehazing.

• The aforementioned techniques have complementary properties and their advantages are combined by the image fusion method to improve the dehazing accuracy.

• The experimental results demonstrate that our method outperforms recent algorithms in real-world haze datasets.

2. Related Work

Dehazing. Dehazing has been widely studied based on the haze model [35], because high-level vision systems requires an ideal environment such as clean weather to perform properly. Conventional dehazing methods were mainly based on image processing and implemented by directly processing pixels or using hand-crafted priors [4, 9, 15, 16, 21, 41]. Various smoothing filters [16, 41] have been also researched because the transmission map in the haze model should be smooth. Tarel *et al*. [41] presented a representative method on smoothing filters. Ancuti *et al*. [4] proposed a semi-inverse method that can deal with pixel intensities of haze regions. For prior-based approaches, DCP [21], color-line prior [16], and haze-line prior [9] have been studied. After dehazing using random forest [51] has been introduced, learning-based methods have been researched. Ancuti *et al*. [2] proposed a multi-scale fusion method using laplacian pyramid. 3C [3] presented a color compensation approach that has some strong points for nighttime dehazing and underwater image enhancement.

While deep learning-based dehazing methods have not been easily proposed due to the lack of datasets, DehazeNet [10] synthesized haze regions using the haze model, estimated the transmission map based on the synthesized dataset, and succeeded in recovering haze-free images through the atmosphere scattering model. This is the firstly proposed end-to-end model for dehazing. Similarly, MSCNN [39] proposed a coarse-to-fine dehazing method by constructing a multi-scale convolution network. AOD-Net [25] estimated transmission and atmospheric light by reformulating the atmosphere scattering model, and directly produced haze-free images without recovering through the haze model. GDN [32] showed high performance by applying an attention-based grid network. FFANet [36] improved the performance without using priors or haze models. DM2F-Net [12] conducted multi-model fusion of multiple results obtained by various layer separation techniques. Dehazing methods in [13, 17, 22, 30, 37] utilized generative adversarial networks. DehazeFlow [27] was the first study to apply the flow model. AECR-Net [44] showed good performance by introducing contrastive learning. DeHamer [20] proposed a transformer-based method that can consider the dark channel. [24] proposed unified model for multi-weather visibility restoration. In contrast to recent methods that are mainly based on deep learning, we argue that traditional image processing-based approaches can help improve the performance of these deep learning-based methods.

Retinex and Curve Adjustment. Curve adjustment and retinex-based methods are typically used for low-light enhancement and image enhancement [19, 28, 34, 38, 43, 45]. Single-scale retinex (SSR), multi-scale retinex with color restoration [38], and structure-based methods [28, 45] have been proposed. The methods in [18, 29] considered the relationship between retinex and dehazing. Owing to the representation power of deep learning, RetinexNet [43] has shown good performance with the fact that the reflectance component of the low-light image and the normal light image are the same. The curve adjustment has been used from gamma curves to commercial photo editing pro-

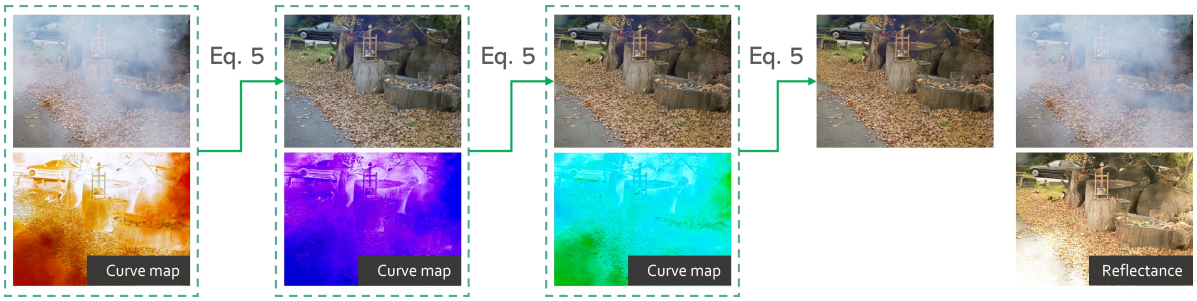

(a) Simple process of dehazing using curve adjustment (b) Retinex decomposition

Figure 2. **Examples of estimated curve maps and reflectance components.** For visualization, we combine three curve maps of the RGB channels into one image in (a). The first curve map recognizes the fog area that needs to be adjusted. As the adjustment is repeated, it becomes closer to the clean image. Reflectance in (b) shows the intrinsic content behind the haze.

grams. CURL [34] directly applied the curve adjustment to deep neural networks. Zero-DCE [19] estimated pixel-wise curves and applied them to low-light image enhancement. In contrast, we improve the dehazing performance using simplified retinex and curve adjustment models.

Other Image Processing Techniques. Before deep learning, most dehazing methods used image processing techniques. The dark channel prior [21] had a block effect problem because the transmission map was estimated using local patches. To solve this problem, image matting techniques have been proposed. In addition, classical median filter was improved and the median of median along lines filter was applied to dehazing by [41]. Color-line [16] and haze-line [9] added smoothing terms to refine the transmission map obtained by the prior. Kim *et al*. [23] introduced low-light enhancement techniques for dehazing to solve the darkening problem of dehazing. The aforementioned methods commonly adopted conventional image processing techniques to solve several problems occurred in the process of dehazing. In this paper, we show that image processing is also competitive to recent deep learning methods.

3. Proposed Methods

We explain each module of the proposed method. Supplementary materials include the detailed network.

3.1. Feature Extraction Module

The feature extraction module (FEM) is used for extracting features of hazy images. For precise feature extraction, we adopt a key component that shows high performance in dehazing (FFANet) and super-resolution (RCAN). This module consists of feature attention blocks which use dual residual connection, channel attention of layers, and pixel attention sequentially. Fig.1 depicts the FEM, in which the residual group consists of five feature attention blocks. Unlike FFANet and RCAN, the proposed FEM has an encoder-decoder architecture:

$$FE(x) = FEM(I(x)), \tag{2}$$

where the extracted feature FE is obtained by passing the hazy image $I(x)$ through the FEM module. The extracted feature map FE in (2) is used as an input for the following direct learning, curve adjustment, retinex decomposition, and fusion modules.

3.2. Direct Learning

Direct learning uses the network output without applying additional image processing techniques. For this, we pass the extracted feature map FE through simple convolution layers (conv-relu-conv-tanh in Fig.1) and adapt the global skip connection, as follows.

$$J^d(x) = D(FE(x)) + I(x), \tag{3}$$

where $D(\cdot)$ is a direct learning function and $J^d(x)$ is the dehazing result produced by direct learning. Direct learning prevents curve adjustment and retinex decomposition from changing dehazing results significantly, thus inducing stable performance.

3.3. Curve Adjustment

Based on the success of curve control for image enhancement and low-light enhancement, we propose a curve adjustment method for dehazing. Zero-DCE [19] illustrates important elements of image adjustment using curve maps. This can be applied to deep learning-based curve adjustment algorithms, while the proposed method also follows this method. The curve is designed as a very simple quadratic curve, considering that the distribution of data should be differentiable, as follows.

$$J^c(x) = I(x) + C(FE(x))I(x)(1 - I(x)), \tag{4}$$

where the dehazing result $J^c(x)$ is obtained using the curve map C with values between -1 and 1, the input image $I(x)$ has values between 0 and 1, and x is the pixel coordinate.

We can apply curves globally to all pixels to prevent loss of data. However, if the curve is adjusted globally, a specific area becomes excessively dark or the brightness of the surrounding area becomes similar, which induces saturation problems. Similarly, adjusting only one curve for

(a) Haze image (b) Direct learning (c) Curve (d) Retinex (e) $J(x)$

Figure 3. **Areas activated by the fusion method for each dehazing component.** (b), (c), and (d) represent individual terms of Eq. (8).

three RGB channels can cause color distortion and make the ratio of pixel color to collapse. In contrast, the proposed curve map C is separately estimated for each channel and each pixel. Since curve maps are learned by comparing the recovered image J with ground-truth, we can obtain curve functions per pixel where saturation and distortion are suppressed. Thus, the curve map is suitable for non-homogeneous dehazing, where the distribution of haze is not uniform. Similar to the direct learning method, the estimated feature from the FEM passes through a simple convolution layer to obtain three curve maps with three channels. The layers consist of Conv-ReLU-Conv-Tanh, as shown in Fig.1. We perform the aforementioned process in an iterative manner, as follows.

$$J_n^c(x) = J_{n-1}^c(x) + C_n(x)J_{n-1}^c(x)(1 - J_{n-1}^c(x)), \quad (5)$$

where the n-th dehazing result $J_n^c(x)$ is obtained using the n-th curve map C_n and the previous dehazing result $J_{n-1}^c(x)$. Fig.2(a) shows estimated curve maps and the proposed dehazing process.

3.4. Retinex Decomposition

Retinex decomposition has been typically used in low-light enhancement, where an clean image is divided into illumination and reflectance components. Like the retinex theory, we assume that the dehazing (clean) image $J^r(x)$ can be divided into the input haze (illumination) image $I(x)$ and reflectance components $R(FE(x))$, as follows.

$$J^r(x) = I(x) \times R(FE(x)), \quad (6)$$

where haze regions can be considered as bright regions in an image, as illumination indicates the brightness of the image. The reflectance component contains intrinsic characteristics of the image regardless of different illumination conditions. Similar to direct learning and curve adjustment, the extracted feature is passed through layers consisting of conv-relu-conv-tanh in Fig.1. Fig.2(b) shows the decomposition results according to the retinex theory, where we can identify the intrinsic content that exists behind the haze region through the reflectance image. This helps remove haze regions and restores content details.

3.5. Multi-Dehazed Image Fusion

The multi-focus image fusion methods [48–50] aim to achieve the proper focus on all subjects in the scene by combining differently focused images. Our method produces three intermediate dehazing results using direct learning, curve adjustment, and retinex decomposition, which are explained in the previous sections. Each result is obtained by each individual network and has different but complementary properties. The proposed method combines these complementary results using multi-focus image fusion for more accurate dehazing. For this, we adopt a simple but powerful multi-focus image fusion method in [50] and generate the fusion map $F(x)$, as follows.

$$F(x) = Softmax(Conv(ReLU(Conv(FE(x))))). \quad (7)$$

Unlike gradient-based or segmentation-based methods, the fusion map can be easily estimated through Conv-ReLU-Conv-2D Softmax. The 2D Softmax function makes our method easy to determine the regions that should be combined. Then, the proposed method combines three dehazing results, $J^d(x)$ in (3), $J^c(x)$ in (5), and $J^r(x)$ in (6) using the corresponding fusion maps, F_1, F_2, and F_3, respectively. $F(x)$ has n channels as many as the number of multi-dehazed images that require fusion.

$$J(x) = F_1 \times J^d(x) + F_2 \times J^c(x) + F_3 \times J^r(x), \quad (8)$$

where the final accurate dehazing result $J(x)$ is obtained by the image fusion. Fig.3 shows the dehazing results activated by fusion maps F_1, F_2, and F_3 for each dehazing component. Using this multi-dehazed image fusion method, a more accurate dehazing result, $J(x)$, can be obtained.

3.6. Loss Function

The integrated loss function of the proposed method is formulated as follows.

$$\mathcal{L}_{total} = \lambda_1(\mathcal{L}_d + \mathcal{L}_c + \mathcal{L}_r) + \lambda_2\mathcal{L}_p + \lambda_3\mathcal{L}_{ssim}, \quad (9)$$

where λ_1, λ_2, and λ_3 balance reconstruction, perceptual, and structural similarity loss terms, respectively. $\mathcal{L}_d$, $\mathcal{L}_c$, and $\mathcal{L}_r$ are L1 losses between the dehazing output of each module of the proposed method and the ground-truth image, respectively. λ_1 and λ_3 were set to 0.5 and λ_2 was set to 1. The perceptual loss learns the similarity between the final dehazing result after the fusion process, $DIP(I)$, and ground-truth, J_{gt}, in the feature domain:

$$\mathcal{L}_p = \|\phi(DIP(I)) - \phi(J_{gt})\|_1, \quad (10)$$

where $\phi(\cdot)$ extracts the 16-th feature map obtained by VGG-16 [40] pretrained using ImageNet [11]. $\mathcal{L}_{ssim}$ measures the structural similarity between $DIP(I)$ and J_{gt} [42].

Table 1. **Quantitative comparison using the SOTS-indoor, SOTS-outdoor, Dense-Haze, and NH-HAZE datasets** in terms of PSNR and SSIM. Red and blue numbers denote the best and second-best results, respectively.

Methods	SOTS-indoor		SOTS-outdoor		Dense-Haze		NH-HAZE	
	PSNR	SSIM	PSNR	SSIM	PSNR	SSIM	PSNR	SSIM
DCP [21]	16.61	0.855	19.14	0.861	11.01	0.416	12.72	0.442
DehazeNet [10]	19.82	0.821	27.75	0.927	9.48	0.438	11.76	0.399
AODNet [25]	20.51	0.816	24.14	0.920	12.82	0.468	15.69	0.573
GDN [32]	32.16	0.984	30.86	0.982	14.96	0.533	18.33	0.667
FFANet [36]	36.39	0.988	33.57	0.984	12.22	0.444	18.13	0.647
AECR-Net [44]	37.17	0.990	-	-	15.80	0.466	19.88	0.717
DeHamer [20]	36.63	0.988	35.18	0.986	16.62	0.560	20.66	0.684
Ours	39.31	0.994	34.72	0.989	17.08	0.601	19.91	0.679

Table 2. **Quantitative comparison with NTIRE challenge winners using SOTS-indoor and NH-HAZE21 datasets** in terms of PSNR and SSIM. The best results are written in boldface.

Methods	SOTS-indoor		NH-HAZE21	
	PSNR	SSIM	PSNR	SSIM
TDN [31]	34.59	0.975	20.23	0.763
TBD [46]	37.61	0.991	21.66	0.843
DW-GAN [17]	35.94	0.986	21.99	0.856
Ours	**39.31**	**0.994**	**23.15**	**0.865**

4. Experiments

The proposed method was implemented by Pytorch and experimented on the NVIDIA RTX 3090 GPU. The initial learning rate was set to 0.0001 and the learning rate was reduced through the cosine annealing strategy. We randomly cropped and used patches with the size of 240×240, thus the original image size did not affect the training procedure. We performed additional data augmentation via horizontal and vertical flips. We used Dense-Haze, NH-HAZE, and NH-HAZE21 datasets for training, while the NTIRE challenge allowed external data.

RESIDE [26] is a synthetic haze dataset that is widely used for dehazing, which can be divided into SOTS-indoor (ITS) and SOTS-outdoor (OTS) datasets. The test set of SOTS had 500 images for both the interior and exterior. The NTIRE challenge dataset contained O-HAZE [8], I-HAZE [1], Dense-Haze [5], NH-HAZE [6], and NH-HAZE21 [7]. We experimented with the Dense-Haze, NH-HAZE, and NH-HAZE21 datasets. Other datasets were too high-resolution to be inferred in a single GPU. In many images, even humans could not recognize contents due to the heavy haze regions. Dense-Haze and NH-HAZE datasets have 45 training images, 5 validation images, and 5 test images. For fair evaluation about NH-HAZE21, we set experimental environments to be similar to the challenge environment. Because the test set was not disclosed at that time, the 21-th to 25-th images out of 25 pair images were tested as the validation set, as in DW-GAN [17] and TBD [46]. Because external data can be used, remaining NTIRE challenge datasets except for O-HAZE and I-HAZE were learned together.

4.1. Comparison with Other Methods

Table 1 quantitatively compared the proposed method with state-of-the-art dehazing methods, DehazeNet [10], AODNet [25], GridDehazeNet [32], FFANet [36], AECR-Net [44], and DeHamer [20]. We used dehazing results reported in the original papers for compared methods. As shown in the table, the proposed method considerably outperformed other methods in the SOTS dataset. Our method significantly improved the dehazing accuracy in terms of SSIM from 0.988 to 0.994. In terms of the PSNR, the proposed method achieved 3 dB improvement compared to DeHamer [20], which is the most recent dehazing method based on the transformer architecture. FFANet [36] produced comparable dehazing results. In SOTS-outdoor, the proposed method produced the highest SSIM scores, while DeHamer produced the highest PSNR scores. However, the transformer network of DeHamer needed to be modified for dehazing, which could induce cropping issues during the test process. Thus, there may be some differences in actual performance. Figs.4 and 5 show qualitative dehazing results on the SOTS-outdoor and indoor datasets, respectively. Because the qualitative performance of compared methods has been already saturated, there is no significant difference in visual quality. Nevertheless, as shown in the red and yellow boxes, our method removed haze regions accurately.

Table 1 and Fig.6 show the results of the NTIRE challenge dataset, Dense-HAZE and NH-HAZE. Dense-HAZE has the heaviest haze density of all existing datasets, and it is difficult to recognize the content behind the haze even by humans. Therefore, the compared methods in Table 1 typically have very low PSNR and SSIM values. Nevertheless, the proposed method exceeds 17 dB in terms of PSNR and 0.6 in terms of SSIM. DeHamer [20] showed the second-best performance because it is the latest method using the transformer architecture. We qualitatively compared the proposed method with the second-best method, DeHamer in Fig.6. As shown in the first row of Fig.6(c), the proposed method produced a more colorful result in the Dense-HAZE dataset. DeHamer could consider long-range dependency and qualitatively showed the best performance in the NH-HAZE dataset with non-homogeneous haze. The proposed method also exhibited high performance.

(a) Haze image (b) DehazeNet [10] (c) AOD-Net [25] (d) GDN [32]

(e) FFANet [36] (f) DeHamer [20] (g) Ours (h) GT

Figure 4. **Qualitative comparison using the SOTS-outdoor dataset [26].**

(a) Haze image (d) GDN [32] (e) FFANet [36]

(f) DeHamer [20] (g) Ours (h) GT

Figure 5. **Qualitative comparison using the SOTS-indoor dataset [26].**

Table 3. **Quantitative comparison using the real-world dataset [16]** in terms of NIQE [33]. The bold numbers denote the best result.

	Color-line [16]	DehazeNet [10]	MSCNN [39]	AOD-Net [25]	GridDehazeNet [32]	FFANet [36]	DeHamer [20]	Ours
NIQE	3.33	3.33	3.32	3.44	3.27	3.29	3.27	**3.23**

Table 2 and Fig.7 show quantitative and qualitative dehazing results on the NH-HAZE21 dataset, respectively. TBD [46], DW-GAN [17], and TDN [31] are NTIRE 2020, NTIRE 2021 winners, and NTIRE 2021 runner-up, respectively. These algorithms produced good results especially for non-homogeneous haze images. Furthermore, the overall performance using other datasets was also good. In particular, TBD [46] showed very high performance on the SOTS-indoor dataset. As shown in Table 2, the proposed method considerably outperformed other state-of-the-art methods. To the best of our knowledge, our method firstly exceeded 23dB in terms of PSNR in the NH-HAZE21 dataset. In Fig.7, DW-GAN restored the block portion of the floor accurately via adversarial learning. The proposed method also produced clear and detailed results. More results can be found in the supplementary materials.

(a) Haze image (b) DeHamer [20] (c) Ours (d) GT

Figure 6. **Qualitative comparison using the NTIRE challenge datasets.** First row: Dense-HAZE [5], Second row: NH-HAZE [6].

(a) Haze image (b) DW-GAN [17] (c) Ours (d) GT

Figure 7. **Qualitative comparison using the NH-HAZE21 dataset [7].**

(a) Input (b) GDN [32] (c) FFANet [36] (d) DeHamer [20] (e) Ours

Figure 8. **Qualitative comparison using the Fattal dataset [16].**

4.2. Experiments on Real-World Haze Images

Characteristics of real-world haze images are very different from those of synthesized haze images. Thus, it is difficult to achieve high-quality results for these images using RESIDE or NTIRE challenge datasets. The existing real-world haze dataset does not have ground-truth and the

(a) Haze image (b) Curve1 (c) Curve3 (d) Curve5

Figure 9. **Ablation study: Dehazing results according to the number of output channels of curve adjustment.**

Table 4. **Ablation study: component-wise evaluation** using the NH-HAZE21 dataset. C, R, and D indicate curve adjustment, retinex decomposition, and direct learning, respectively. The best results are written in boldface.

	C	R + D	C + D	C + R	Full model
PSNR	19.69	22.23	21.84	22.34	**23.15**

(a) Input (b) Curve adjustment

Figure 10. **Limitations of curve adjustment on heavy haze.**

characteristics of haze regions are very different for different image data. The RESIDE dataset has various landscapes. However, it was captured by a single camera and had limited areas. Thus, image data have a similar tone. The NTIRE challenge datasets include very dense and non-homogeneous haze regions. In addition, the number of data is less than 50 and the average color is biased toward blush. Thus, this dataset does not represent a common haze situation. Therefore, for real-world haze removal, we used a dataset synthesized by the haze model in the VOC2007 dataset [14], which contains various colors and diverse objects. However, the dehazing methods in [10, 25, 39] using haze datasets synthesized by the haze model have a darkening problem after haze removal. To solve this problem, we introduce a cutHaze method based on cutMix [47], in which a part of the clean image is pasted into the haze image as training data. Table 3 shows quantitative dehazing results in terms of the no-reference image quality metric, NIQE [33]. The proposed method produced the most accurate results. Fig.8 shows the corresponding qualitative results. FFANet and DeHamer, which showed high performance on other datasets, showed inaccurately removed haze regions in the real-world dataset. In contrast, our method produced clear and high-quality results compared to other algorithms.

4.3. Ablation Study

Table 4 analyzed the contribution of each module of the proposed method. If only the curve adjustment is used, curve mapping is performed for each pixel, and haze areas are inferred roughly. However, due to the nature of the NH-HAZE dataset, it is difficult to process dense areas. By employing direct learning (*i.e.* R + D and C + D), the proposed method could produce more accurate dehazing results, demonstrating the effectiveness of direct learning. C + R also exhibited high performance, indicating that two image processing modules help each other to enhance the dehazing accuracy. When using the full modules, the proposed method could achieve state-of-the-art performance.

Fig.9 shows the dehazing results $J^c(x)$ obtained by the curve adjustment module. Curve1, Curve3, and Curve5 have 3, 9, and 15 output channels for the curve adjustment, respectively. By using Curve5, the proposed method could remove most hazy areas, as shown in Fig.9(d), which demonstrates the contribution of the proposed curve adjustment. However, except for heavy haze areas, there was no significant difference in non-haze areas and in dehazing results when considering the overall combination. Thus, we experimentally used Curve3 for our dehazing method. Fig.10 shows limitations of curve adjustment with heavy haze regions. Despite this limitation, the proposed method could produce accurate dehazing results by fusing intermediate dehazing results based on the multi-fusion method.

5. Conclusion

We proposed a dehazing method that can demonstrate high performance using incorporating a network with image processing techniques. We introduced the direct learning method, mainly used in deep learning, curve adjustment, retinex theory, and image fusion method. The experimental results demonstrated that the proposed method quantitatively and qualitatively produced accurate dehazing results compared to recent algorithms.

Acknowledgments. This work was partly supported by Seoul Campus Town Technology RD Project (Advanced development of visible/thermal AI monocular depth estimation technology) and was supported by Institute of Information communications Technology Planning Evaluation (IITP) grant funded by the Korea government (MSIT) (No. 2022-0-00926)

References

[1] Cosmin Ancuti, Codruta O Ancuti, Radu Timofte, and Christophe De Vleeschouwer. I-haze: a dehazing benchmark with real hazy and haze-free indoor images. In *ACIVS*, 2018. 5

[2] Codruta Orniana Ancuti and Cosmin Ancuti. Single image dehazing by multi-scale fusion. *IEEE Transactions on Image Processing*, 22(8):3271–3282, 2013. 2

[3] Codruta O Ancuti, Cosmin Ancuti, Christophe De Vleeschouwer, and Mateu Sbert. Color channel compensation (3c): A fundamental pre-processing step for image enhancement. *IEEE Transactions on Image Processing*, 29:2653–2665, 2019. 2

[4] Codruta O Ancuti, Cosmin Ancuti, Chris Hermans, and Philippe Bekaert. Layer-based single image dehazing by per-pixel haze detection. In *ACM SIGGRAPH ASIA 2010 Sketches*. 2010. 2

[5] Codruta O Ancuti, Cosmin Ancuti, Mateu Sbert, and Radu Timofte. Dense-haze: A benchmark for image dehazing with dense-haze and haze-free images. In *ICIP*, 2019. 5, 7

[6] Codruta O Ancuti, Cosmin Ancuti, and Radu Timofte. Nh-haze: An image dehazing benchmark with non-homogeneous hazy and haze-free images. In *CVPR Workshops*, 2020. 5, 7

[7] Codruta O Ancuti, Cosmin Ancuti, and Radu Timofte. Nh-haze: An image dehazing benchmark with non-homogeneous hazy and haze-free images. In *CVPR Workshops*, 2020. 5, 7

[8] Codruta O. Ancuti, Cosmin Ancuti, Radu Timofte, and Christophe De Vleeschouwer. O-HAZE: a dehazing benchmark with real hazy and haze-free outdoor images. In *CVPR Workshops*, 2018. 5

[9] D. Berman, T. Treibitz, and S. Avidan. Non-local image dehazing. In *CVPR*, 2016. 1, 2, 3

[10] Bolun Cai, Xiangmin Xu, Kui Jia, Chunmei Qing, and Dacheng Tao. DehazeNet: An end-to-end system for single image haze removal. *IEEE TIP*, 25(11):5187–5198, 2016. 2, 5, 6, 8

[11] J. Deng, W. Dong, R. Socher, L.-J. Li, K. Li, and L. Fei-Fei. ImageNet: A Large-Scale Hierarchical Image Database. In *CVPR*, 2009. 4

[12] Zijun Deng, Lei Zhu, Xiaowei Hu, Chi-Wing Fu, Xuemiao Xu, Qing Zhang, Jing Qin, and Pheng-Ann Heng. Deep multi-model fusion for single-image dehazing. In *ICCV*, 2019. 2

[13] Yu Dong, Yihao Liu, He Zhang, Shifeng Chen, and Yu Qiao. Fd-gan: Generative adversarial networks with fusion-discriminator for single image dehazing. In *AAAI*, 2020. 2

[14] Mark Everingham, Luc Van Gool, Christopher KI Williams, John Winn, and Andrew Zisserman. The pascal visual object classes (voc) challenge. *International journal of computer vision*, 88(2):303–338, 2010. 8

[15] Raanan Fattal. Single image dehazing. *ACM TOG*, 27(3):1–9, 2008. 1, 2

[16] Raanan Fattal. Dehazing using color-lines. *ACM TOG*, 34(13):13:1–13:14, 2014. 1, 2, 3, 6, 7

[17] Minghan Fu, Huan Liu, Yankun Yu, Jun Chen, and Keyan Wang. Dw-gan: A discrete wavelet transform gan for non-homogeneous dehazing. In *CVPR Workshops*, 2021. 2, 5, 6, 7

[18] Adrian Galdran, Aitor Alvarez-Gila, Alessandro Bria, Javier Vazquez-Corral, and Marcelo Bertalmío. On the duality between retinex and image dehazing. In *CVPR*, 2018. 2

[19] Chunle Guo Guo, Chongyi Li, Jichang Guo, Chen Change Loy, Junhui Hou, Sam Kwong, and Runmin Cong. Zero-reference deep curve estimation for low-light image enhancement. In *CVPR*, 2020. 1, 2, 3

[20] Chun-Le Guo, Qixin Yan, Saeed Anwar, Runmin Cong, Wenqi Ren, and Chongyi Li. Image dehazing transformer with transmission-aware 3d position embedding. In *CVPR*, 2022. 1, 2, 5, 6, 7

[21] Kaiming He, Jian Sun, and Xiaoou Tang. Single image haze removal using dark channel prior. In *CVPR*, 2009. 1, 2, 3, 5

[22] Ziling Huang, Qili Deng, Chung-Chi Tsai, and Chia-Wen Lin. Hardgan: A haze-aware representation distillation gan for single image dehazing. In *ECCV*, 2020. 2

[23] Guisik Kim and Junseok Kwon. Deep illumination-aware dehazing with low-light and detail enhancement. *IEEE TITS*, 23(3):2494–2508, 2021. 3

[24] Ashutosh Kulkarni, Prashant W Patil, Subrahmanyam Murala, and Sunil Gupta. Unified multi-weather visibility restoration. *IEEE Transactions on Multimedia*, 2022. 2

[25] Boyi Li, Xiulian Peng, Zhangyang Wang, Jizheng Xu, and Dan Feng. AOD-Net: All-in-one dehazing network. In *ICCV*, 2017. 2, 5, 6, 8

[26] Boyi Li, Wenqi Ren, Dengpan Fu, Dacheng Tao, Dan Feng, Wenjun Zeng, and Zhangyang Wang. Reside: A benchmark for single image dehazing. *arXiv preprint arXiv:1712.04143*, 1, 2017. 5, 6

[27] Hongyu Li, Jia Li, Dong Zhao, and Long Xu. Dehazeflow: Multi-scale conditional flow network for single image dehazing. In *ACM Multimedia*, 2021. 1, 2

[28] Mading Li, Jiaying Liu, Wenhan Yang, Xiaoyan Sun, and Zongming Guo. Structure-revealing low-light image enhancement via robust retinex model. *IEEE TIP*, 27(6):2828–2841, 2018. 1, 2

[29] Pengyue Li, Jiandong Tian, Yandong Tang, Guolin Wang, and Chengdong Wu. Deep retinex network for single image dehazing. *IEEE TIP*, 30:1100–1115, 2020. 2

[30] Runde Li, Jinshan Pan, Zechao Li, and Jinhui Tang. Single image dehazing via conditional generative adversarial network. In *CVPR*, 2018. 2

[31] Jing Liu, Haiyan Wu, Yuan Xie, Yanyun Qu, and Lizhuang Ma. Trident dehazing network. In *CVPR Workshops*, 2020. 5, 6

[32] Xiaohong Liu, Yongrui Ma, Zhihao Shi, and Jun Chen. Griddehazenet: Attention-based multi-scale network for image dehazing. In *ICCV*, 2019. 2, 5, 6, 7

[33] Anish Mittal, Rajiv Soundararajan, and Alan C Bovik. Making a "completely blind" image quality analyzer. *IEEE Signal processing letters*, 20(3):209–212, 2012. 6, 8

[34] Sean Moran, Steven McDonagh, and Gregory Slabaugh. Curl: Neural curve layers for global image enhancement. In *ICPR*, 2021. 1, 2, 3

[35] Shree K Nayar and Srinivasa G Narasimhan. Vision in bad weather. In *ICCV*, 1999. 2

[36] Xu Qin, Zhilin Wang, Yuanchao Bai, Xiaodong Xie, and Huizhu Jia. Ffa-net: Feature fusion attention network for single image dehazing. In *AAAI*, 2020. 2, 5, 6, 7

[37] Yanyun Qu, Yizi Chen, Jingying Huang, and Yuan Xie. Enhanced pix2pix dehazing network. In *CVPR*, 2019. 2

[38] Zia-ur Rahman, Daniel J Jobson, and Glenn A Woodell. Multi-scale retinex for color image enhancement. In *ICIP*, 1996. 1, 2

[39] Wenqi Ren, Si Liu, Hua Zhang, Jinshan Pan, Xiaochun Cao, and Ming-Hsuan Yang. Single image dehazing via multi-scale convolutional neural networks. In *ECCV*, 2016. 2, 6, 8

[40] Karen Simonyan and Andrew Zisserman. Very deep convolutional networks for large-scale image recognition. *arXiv preprint arXiv:1409.1556*, 2014. 4

[41] Jean-Philippe Tarel and Nicolas Hautiere. Fast visibility restoration from a single color or gray level image. In *ICCV*, 2009. 1, 2, 3

[42] Zhou Wang, Alan C Bovik, Hamid R Sheikh, and Eero P Simoncelli. Image quality assessment: from error visibility to structural similarity. *IEEE TIP*, 13(4):600–612, 2004. 4

[43] Chen Wei, Wenjing Wang, Wenhan Yang, and Jiaying Liu. Deep retinex decomposition for low-light enhancement. *arXiv preprint arXiv:1808.04560*, 2018. 1, 2

[44] Haiyan Wu, Yanyun Qu, Shaohui Lin, Jian Zhou, Ruizhi Qiao, Zhizhong Zhang, Yuan Xie, and Lizhuang Ma. Contrastive learning for compact single image dehazing. In *CVPR*, 2021. 2, 5

[45] Jun Xu, Yingkun Hou, Dongwei Ren, Li Liu, Fan Zhu, Mengyang Yu, Haoqian Wang, and Ling Shao. Star: A structure and texture aware retinex model. *IEEE TIP*, 29:5022–5037, 2020. 1, 2

[46] Yankun Yu, Huan Liu, Minghan Fu, Jun Chen, Xiyao Wang, and Keyan Wang. A two-branch neural network for non-homogeneous dehazing via ensemble learning. In *CVPR*, 2021. 5, 6

[47] Sangdoo Yun, Dongyoon Han, Seong Joon Oh, Sanghyuk Chun, Junsuk Choe, and Youngjoon Yoo. Cutmix: Regularization strategy to train strong classifiers with localizable features. In *Proceedings of the IEEE/CVF international conference on computer vision*, pages 6023–6032, 2019. 8

[48] Hao Zhang, Zhuliang Le, Zhenfeng Shao, Han Xu, and Jiayi Ma. Mff-gan: An unsupervised generative adversarial network with adaptive and gradient joint constraints for multi-focus image fusion. *Information Fusion*, 66:40–53, 2021. 4

[49] Hao Zhang, Han Xu, Yang Xiao, Xiaojie Guo, and Jiayi Ma. Rethinking the image fusion: A fast unified image fusion network based on proportional maintenance of gradient and intensity. In *AAAI*, 2020. 4

[50] Xingchen Zhang. Multi-focus image fusion: A benchmark. *arXiv preprint arXiv:2005.01116*, 2020. 1, 4

[51] Qingsong Zhu, Jiaming Mai, and Ling Shao. Single image dehazing using color attenuation prior. In *BMVC*, 2014. 2